Available online at www.sciencedirect.com
ScienceDirect
Journal of Solid State Chemistry 180 (2007) 3381–3387
JOURNAL OF SOLID STATE CHEMISTRY
www.elsevier.com/locate/jssc

Synthesis, structure and X-ray excited luminescence of Ce^{3+}-doped $AREP_2O_7$-type alkali rare earth diphosphates (A = Na, K, Rb, Cs; RE = Y, Lu)

Jun-Lin Yuan[a,b], Hui Zhang[a], Hao-Hong Chen[a], Xin-Xin Yang[a], Jing-Tai Zhao[a,*], Mu Gu[c]

[a]*State Key Laboratory of High Performance Ceramics and Superfine Microstructure, Shanghai Institute of Ceramics, Chinese Academy of Sciences, Shanghai 200050, PR China*
[b]*Graduate School of Chinese Academy of Sciences, Beijing, PR China*
[c]*Tongji University, Shanghai 200020, PR China*

Received 2 June 2007; received in revised form 4 September 2007; accepted 6 September 2007
Available online 26 September 2007

Abstract

The crystal structures of five new alkali rare earth diphosphates were obtained by Rietveld refinement of powder X-ray diffraction (XRD) profiles, including four alkali lutetium diphosphates $ALuP_2O_7$ (A = Na, K, Rb, Cs) and the low temperature phase of KYP_2O_7. The scintillation properties of Ce^{3+}-doped $AREP_2O_7$ (A = Na, K, Rb, Cs; RE = Y, Lu) powder samples were studied under static and pulsed X-ray excitations, and featured outstanding scintillation properties with light yields 1–2 times of that of $Bi_4(GeO_4)_3$ and relatively short decay time of 20–28 ns. Considering the suitable emission wavelength range, large light yield, short decay time, and non-hygroscopic nature, Ce^{3+}-doped $AREP_2O_7$-type alkali rare earth diphosphates are potential candidates for high-counting-rate scintillation applications.

Keywords: Alkali rare earth diphosphates; Rietveld refinement; X-excited luminescence

1. Introduction

Recently, investigation of the synthesis and characterization of alkali rare earth phosphates has gained much attention due to their potential applications in diverse areas such as X-ray and gamma-radiation scintillators [1,2], lighting, display phosphors [3], solid-state lasers [4], catalysts and ion conductors [5]. $AREP_2O_7$ (A = alkali, RE = rare earth) type alkali rare earth diphosphate is an important member in the A_2O–RE_2O_3–P_2O_5 ternary system, of which previously the major attention was concentrated on structural investigations. Among the numerous diphosphates $A^{I}M^{III}P_2O_7$ (A = alkali, Ag, Tl; M = Al, Ga, RE, transition metal), at least 8 structural types have been reported [5,6]. For alkali rare earth diphosphates $AREP_2O_7$ with large A^+ and small RE^{3+} (r_A/r_M = 1.51–2.73), the structure type corresponds to the $KAlP_2O_7$ type with S. G. of $P2_1/c$ (No.14) and Z equals 4 in each unit cell. As for smaller alkali ion (such as Li^+ and Na^+) with smaller r_A/r_M ratio, several other structural types were identified: $LiScP_2O_7$ in $P2_1$ (No. 14) with Z = 2 [5], $NaYP_2O_7$ in $P2_1$ (No. 4) with Z = 4 [7], $NaYbP_2O_7$ in $P2_1/n$ (No. 14) with Z = 4 [8], and $NaLnP_2O_7$ (Ln = La–Ce) in $Pnma$ (No. 62) with Z = 4 [9]. However, alkali rare earth diphosphates with r_A/r_M ratio near the lower limit (1.51) always show transitional structure types, for example, KYP_2O_7 crystals grown from high temperature melt show S. G. of $Cmcm$ (No. 63) with Z = 4 [10]. Nevertheless, since the r_K^+/r_Y^{3+} ratio (1.68) is in the range of 1.51–2.73 mentioned above, KYP_2O_7 should have a low temperature phase of $KAlP_2O_7$-type structure. In this work, the low temperature phase of KYP_2O_7 was obtained at a lower temperature. For convenience, the high temperature phase and low temperature phase were titled as α-KYP_2O_7 and β-KYP_2O_7, respectively. Besides, the four alkali lutetium diphosphates $ALuP_2O_7$ (A = Na–Cs) is first reported here

*Corresponding author. Fax: +86 021 52413122.
E-mail address: jtzhao@mail.sic.ac.cn (J.-T. Zhao).

0022-4596/$ - see front matter © 2007 Elsevier Inc. All rights reserved.
doi:10.1016/j.jssc.2007.09.021

and their structures were obtained via powder XRD Rietveld refinement. It was found that β-KYP_2O_7 and $ALuP_2O_7$ (A = K–Cs) features the $KAlP_2O_7$-type structure, and $NaLuP_2O_7$ is isostructural with $NaYbP_2O_7$.

Due to the wide band gap and the suitability for doping with rare earth activators, the luminescent properties of alkali rare earth phosphates under VUV and X-ray radiation were widely reported in the last several years, though most of the studies were concentrated on the $A_3RE(PO_4)_2$-type alkali rare earth phosphates. For example, $Na_3RE(PO_4)_2$, $K_3Lu(PO_4)_2$, $Rb_3Lu(PO_4)_2$, and $Cs_3Lu(PO_4)_2$, among which Ce^{3+}-doped $A_3Lu(PO_4)_2$ (A = K, Rb, Cs) were identified as promising fast scintillators [1]. However, $A_3RE(PO_4)_2$-type alkali rare earth phosphates are hygroscopic, which restricts their applications. As a comparison, $AREP_2O_7$ are non-hygroscopic since alkali ions are safely encaged by [REO_6] and [P_2O_7] groups. Nevertheless, the optical investigations of the $AREP_2O_7$-type alkali rare earth diphosphates remain insufficient, though Jouini et al. [2] studied the X-ray excited luminescence (XEL) of $NaPrP_2O_7$, and Li et al. [11] reported the XEL of Ce^{3+}-doped $NH_4LuP_2O_7$. We have studied the VUV–UV excited luminescent properties of Ce^{3+}, Pr^{3+}-doped $AREP_2O_7$ (A = Na, K, Rb, Cs; RE = Y, Lu) [12] and Ln^{3+}-doped $NaREP_2O_7$ (Ln = Ce, Pr, Tb, Eu, Tm; RE = La, Gd). In this work, the luminescent spectra of Ce^{3+}-doped α-KYP_2O_7, AYP_2O_7 (A = Rb, Cs) and $ALuP_2O_7$ (A = Na, K, Rb, Cs) under static hard X-ray radiation were presented, and their decay profiles under pulsed hard X-ray radiation were also presented. The series of Ce^{3+}-doped $AREP_2O_7$ alkali rare earth diphosphates features high light yield and fast decay time, which might be potential candidates as fast scintillators [13].

2. Experimental sections

2.1. Sample preparation

Powder samples of $NaLuP_2O_7$, α-KYP_2O_7, β-KYP_2O_7, $KLuP_2O_7$, $RbYP_2O_7$, $RbLuP_2O_7$, $CsYP_2O_7$ and $CsLuP_2O_7$ were prepared by solid-state reactions. Analytical grade reagents, Na_2CO_3, KNO_3, $RbNO_3$, Cs_2CO_3, Y_2O_3, Lu_2O_3, CeO_2, Pr_6O_{11} and $(NH_4)_2HPO_4$, were weighed stoichiometrically, mixed thoroughly in agate mortar, pre-calcined at 400 °C for 1 h in covered alumina crucibles, then reground and subsequently calcined at 750 °C (650 °C for β-KYP_2O_7) for 24 h in covered alumina crucibles. However, when trying to obtain $NaYP_2O_7$ from solid-state reactions, YPO_4 and $NaPO_3$ glass were obtained instead. For Ce^{3+}-doped samples, the doping concentration was 0.5 mol% and the samples were heat treated in mild reducing atmosphere of CO. All of the samples are purely white and non-hygroscopic.

2.2. X-ray diffraction (XRD) analysis

The powder XRD data for phase identification was collected at ambient temperature with a Rigaku D/max2500 diffractometer (Cu$K\alpha$ radiation, 40 kV/200 mA). The XRD patterns of $NaLuP_2O_7$ and three yttrium compounds, α-KYP_2O_7, $RbYP_2O_7$ and $CsYP_2O_7$, match well with the patterns reported in ICDD database (Card No. 41-0418, 49-1161, 49-0122) or calculated from ICSD database. The powder XRD data used for Rietveld refinement were collected with Model X'Pert PRO (PANalytical, Holland, Cu$K\alpha$1 1.54056 Å, X' Celerator Detector) operated at 40 kV and 40 mA (step size of 0.017° and count-time of 2 s/step). In the Rietveld refinement, the atomic positions of $NaYbP_2O_7$ [8] were used as the starting model for $NaLuP_2O_7$, $KAlP_2O_7$ [14] for β-KYP_2O_7 and $KLuP_2O_7$, and $RbYP_2O_7$ [15] for $RbLuP_2O_7$ and $CsLuP_2O_7$, among which $NaYbP_2O_7$ is in S. G. of $P2_1/n$ (No. 14) with $Z = 4$, and the other diphosphates included here are in S. G. of $P2_1/c$ (No. 14) with $Z = 4$.

2.3. Optical measurements

The XEL spectra were measured on an X-ray excited spectrometer, FluoMain, where a F-30 movable clinical X-ray tube (W anticathode target) was used as the X-ray source, and operated under the same conditions (30 kV, 4 mV) at room temperature. The XEL spectra of the samples were obtained by 44 W plate grating monochromator

Table 1
Unit cell parameters and R-factors of $ALuP_2O_7$ and β-KYP_2O_7 obtained from Rietveld refinement of powder XRD data

Compound	$NaLuP_2O_7$	β-KYP_2O_7	$KLuP_2O_7$	$RbLuP_2O_7$	$CsLuP_2O_7$
S. G., Z	$P2_1/n$, 4	$P2_1/c$, 4	$P2_1/c$, 4	$P2_1/c$, 4	$P2_1/c$, 4
a (Å)	9.0277(1)	7.5797(2)	7.5490(1)	7.6797(1)	7.8768(1)
b (Å)	5.3629(1)	10.9371(3)	10.7847(1)	10.7785(1)	10.7282(1)
c (Å)	12.7710(1)	8.5918(2)	8.5394(1)	8.6061(1)	8.7036(1)
β (°)	103.36(0)	106.92(0)	106.69(0)	105.37(0)	104.36(0)
V(Å^3)	601.57(9)	681.44(29)	665.92(16)	686.88(13)	712.51(16)
ρ_{cal}(g cm^{-3})	4.11	2.94	3.87	4.20	4.49
R_p(%)	4.85	6.21	5.15	4.14	4.67
R_{wp}(%)	6.84	9.00	7.57	5.65	6.25
R_{exp}(%)	2.55	5.82	2.62	2.16	3.13

and Hamamatsu R928-28 PMT with the data acquired by computer. The fluorescence lifetimes were measured by exciting the samples with pulsed X-ray (maximal excited energy 30 keV) and detected by a S-1 photomultiplier tube. The time resolution of the X-ray excited fluorescence lifetime is 0.97 ns. All of the measurements were carried out under room temperature.

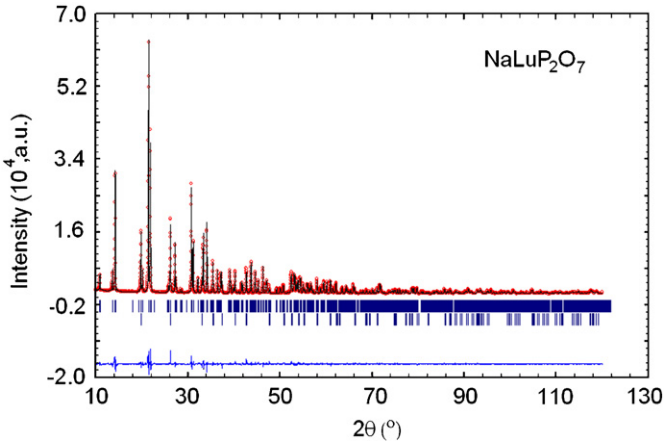

Fig. 1. Observed (dots), calculated (solid line) and difference XRD patterns of $NaLuP_2O_7$. The second row of Brag positions belongs to the second phase $LuPO_4$ with content of 2.7 wt%.

3. Results and discussion

3.1. Structural aspects

Structural refinements were carried out using *FullProf* [16], from which the unit cell parameters and *R*-factors were tabulated in Table 1. The observed, calculated and difference powder XRD patterns of the five $AREP_2O_7$ diphosphates were presented in Figs. 1 and 2, and the atomic positions were tabulated in Tables 2–4. As shown in Figs. 1 and 2, a small amount of second phase of $LuPO_4$ was found in the $NaLuP_2O_7$ sample, and Lu_2O_3 second phase in the $KLuP_2O_7$ and $CsLuP_2O_7$ samples. The correctness of the refinement is indicated by checking the atom distances, from which the P–O distances are in range of 1.457–1.642 Å and the average P–O distances are in the range of 1.522–1.545 Å that are close to 1.54 Å for P–O

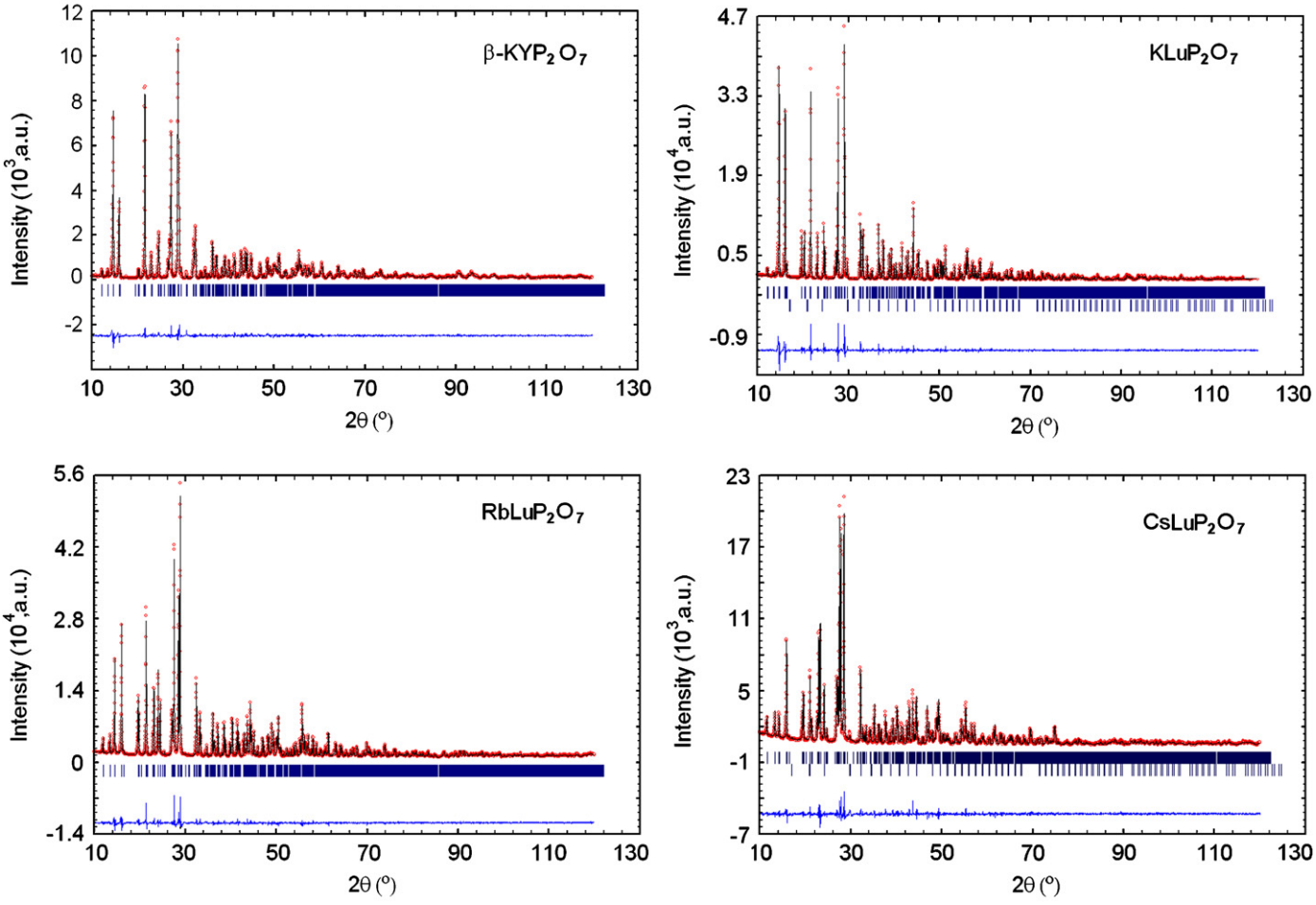

Fig. 2. The observed (dot), calculated (solid line) and difference XRD patterns of β-KYP_2O_7, $KLuP_2O_7$, $RbLuP_2O_7$ and $CsLuP_2O_7$. The second row of Brag positions belongs to the second phase of Lu_2O_3 with content of 1.0 and 1.4 wt% in the samples of $KLuP_2O_7$ and $CsLuP_2O_7$, respectively.

Table 2
Atomic parameters of $NaLuP_2O_7$ obtained from Rietveld refinement

Atom	x/a	y/b	z/c	U_{iso} (Å^2)
Na1	0.6378(8)	0.228(3)	0.1920(6)	0.027(3)
Lu1	0.77057(14)	0.7629(4)	0.02406(9)	0.0086(2)
P1	0.9739(6)	0.251(3)	0.1535(4)	0.0104(17)
P2	0.5670(7)	0.285(2)	0.8816(5)	0.015(2)
O1	0.0614(13)	0.272(5)	0.0668(10)	0.013(4)
O2	0.896(2)	−0.001(4)	0.1622(14)	0.008(6)
O3	0.8635(20)	0.466(4)	0.1491(14)	0.012(6)
O4	0.1009(11)	0.269(4)	0.2679(9)	0.011(4)
O5	0.6771(14)	0.123(2)	0.9531(12)	0.009(5)
O6	0.4066(13)	0.212(4)	0.8754(8)	0.007(5)
O7	0.5992(16)	0.544(3)	0.9092(12)	0.017(5)

Table 3
Atomic parameters of β-KYP_2O_7 and $KLuP_2O_7$ obtained from Rietveld refinement

Atom	x/a	y/b	z/c	U_{iso}[Å^2]
β-KYP_2O_7				
K1	0.1872(5)	0.3216(3)	0.0687(4)	0.0239(11)
Y1	0.2313(2)	0.59522(14)	0.7488(2)	0.0081(3)
P1	0.4479(6)	0.6442(4)	0.1907(6)	0.0116(13)
P2	0.1296(6)	0.8996(4)	0.8066(5)	0.0086(12)
O1	0.3418(11)	0.9206(8)	0.8071(10)	0.021(3)
O2	0.0668(11)	0.7287(9)	0.2387(12)	0.007(3)
O3	0.6305(10)	0.5882(9)	0.2471(11)	0.013(3)
O4	0.1237(13)	0.5964(9)	0.4732(12)	0.020(3)
O5	0.3385(12)	0.6137(8)	0.0185(12)	0.020(3)
O6	1.0158(12)	0.4992(9)	0.2089(9)	0.006(3)
O7	0.4635(11)	0.7777(9)	0.2254(10)	0.004(3)
$KLuP_2O_7$				
K1	0.1822(7)	0.3217(4)	0.0653(7)	0.0287(18)
Lu1	0.23255(20)	0.59734(10)	0.7523(2)	0.0095(2)
P1	0.4466(9)	0.6437(6)	0.1915(9)	0.013(2)
P2	0.1316(8)	0.8987(7)	0.8129(8)	0.0128(19)
O1	0.3418(17)	0.9309(13)	0.8060(17)	0.032(5)
O2	0.0679(19)	0.7350(14)	0.238(2)	0.010(5)
O3	0.6387(14)	0.5893(14)	0.2438(16)	0.013(4)
O4	0.1360(19)	0.5979(14)	0.4855(20)	0.014(5)
O5	0.3313(19)	0.6127(14)	0.0135(19)	0.014(5)
O6	1.0154(19)	0.5009(13)	0.2178(16)	0.020(5)
O7	0.460(2)	0.7773(14)	0.2324(19)	0.017(5)

Table 4
Atomic parameters of $RbLuP_2O_7$ and $CsLuP_2O_7$ obtained from Rietveld refinement

Atom	x/a	y/b	z/c	U_{iso}[Å^2]
$RbLuP_2O_7$				
Rb	0.1911(3)	0.31718(18)	0.0591(3)	0.0187(6)
Lu1	0.23437(16)	0.59868(10)	0.75287(17)	0.0035(2)
P1	0.4390(8)	0.6369(6)	0.1876(7)	0.0129(19)
P2	0.1323(7)	0.8992(6)	0.8162(6)	0.0049(15)
O1	0.3284(14)	0.9331(11)	0.8012(12)	0.017(4)
O2	0.0753(15)	0.7266(11)	0.2559(14)	0.007(4)
O3	0.6208(13)	0.5756(11)	0.2313(13)	0.005(4)
O4	0.1488(17)	0.5900(12)	0.4934(15)	0.019(5)
O5	0.3376(15)	0.6115(11)	0.0176(13)	0.007(4)
O6	0.9935(14)	0.4978(10)	0.2230(12)	0.007(4)
O7	0.4498(15)	0.7741(11)	0.2320(12)	0.007(4)
$CsLuP_2O_7$				
Cs1	0.1986(3)	0.30410(16)	0.0487(2)	0.0158(6)
Lu1	0.23645(20)	0.59984(15)	0.7547(2)	0.0006(3)
P1	0.4257(12)	0.6297(9)	0.1832(11)	0.032(3)
P2	0.1324(10)	0.9034(9)	0.8206(9)	0.013(2)
O1	0.3237(19)	0.9426(13)	0.7929(17)	0.011(5)
O2	0.0748(19)	0.7287(14)	0.2628(17)	0.007(6)
O3	0.6090(19)	0.5723(14)	0.2346(16)	0.014(6)
O4	0.156(2)	0.5825(15)	0.4938(17)	0.010(6)
O5	0.337(2)	0.6029(17)	0.0157(18)	0.024(6)
O6	0.999(2)	0.5046(15)	0.2294(17)	0.021(6)
O7	0.4435(19)	0.7605(14)	0.2242(18)	0.008(6)

[17]. The A–O distances and RE–O distances in the [REO_6] octahedra are normal as well.

$NaLuP_2O_7$ is not isostructural with the other $KAlP_2O_7$-type diphosphates. As shown in Fig. 3a, Na^+ ions locate at a tunnel along the c-axis formed by stacking hexagonal rings of [$Lu_2P_4O_{22}$]. Further analysis indicates that Na^+ ions are encaged in the cage constructed by three hexagonal rings (Fig. 4a). As previously reported in the VUV–UV spectroscopic properties of Ce^{3+}-doped $AREP_2O_7$, the very low value of Stokes shift of Ce^{3+} in $NaLuP_2O_7$ indicates a very stiffness nature of the cage in $NaLuP_2O_7$ [12]. Besides, the Na–O distance the cage is relatively small comparing with the known fast Na^+ conductors [18]. Hence Na^+ ions are confined in the stiff cage and fast ion conduction is not expected.

As for the $KAlP_2O_7$-type diphosphates that constitute the largest structure type in the $A^{I}M^{III}P_2O_7$ ternary system, the basic building block is the tunnel structure formed by septangular rings stacking along the c-axis (Figs. 4b and c). The structure of stacking rings in $KAlP_2O_7$-type diphosphates is validated in the Ce^{3+}-doped UV excited luminescent spectra. Since Stokes shift of Ce^{3+} is an indicator of the stiffness of host lattice, in $KAlP_2O_7$-type diphosphates the larger A^+ and smaller RE^{3+} would brought out smaller Stokes shift [12], indicating the more rigid nature of the $KAlP_2O_7$-type host lattice.

3.2. X-ray excited luminescence of Ce^{3+}-doped $AREP_2O_7$

In the previous paper [12], the VUV spectroscopic properties of $AREP_2O_7$:Ce^{3+} were reported and an efficient host→Ce^{3+} energy transfer was identified, which is crucial for a large light yield of scintillators [19]. The XEL spectra of $AREP_2O_7$:0.5% Ce^{3+} (A = Na, K, Rb, Cs; RE = Y, Lu) powder samples were presented in Fig. 5. Under the excitation of hard X-ray photons, all of the samples show strong emissions in the range of 325–450 nm, which originates from the parity allowed Ce^{3+} $5d$→$4f$($^2F_{5/2}$, $^2F_{7/2}$) radiative transition. The high similarity in the emission spectra of the series of $AREP_2O_7$ verifies their structural and compositional similarity. It should be noted that the observed emission in $NaLuP_2O_7$:Ce sample could

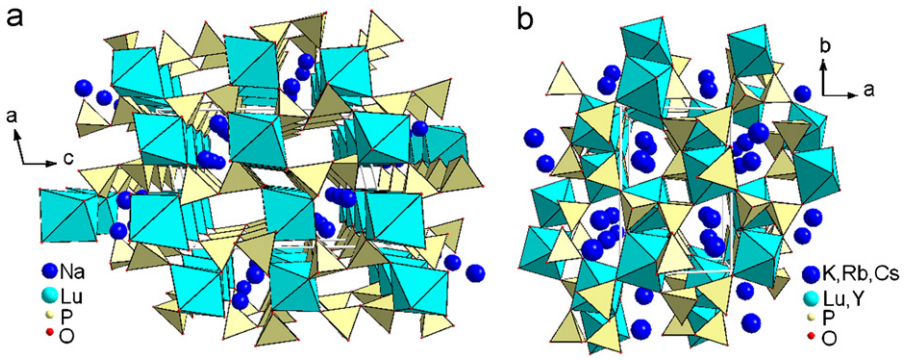

Fig. 3. (a) Perspective view along [010] direction of the crystal structure of $NaLuP_2O_7$, and (b) perspective view along [001] direction of the crystal structure of β-KYP_2O_7, $KLuP_2O_7$, $RbLuP_2O_7$ and $CsLuP_2O_7$ that are isostructural with $KAlP_2O_7$.

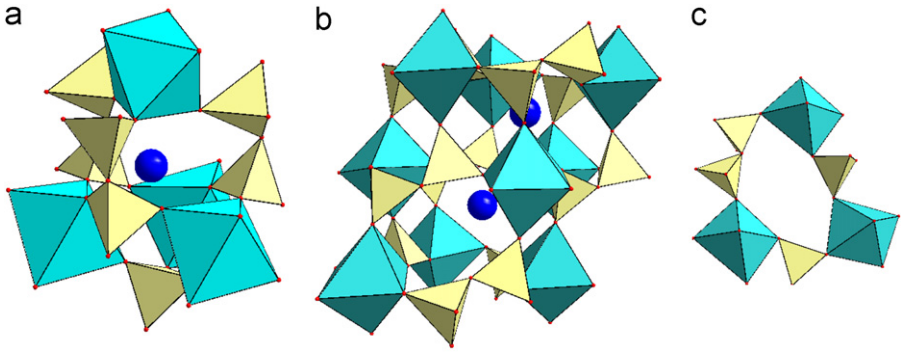

Fig. 4. (a) In $NaLuP_2O_7$, Na^+ ion is encaged in the cage formed by three hexagonal rings of $[Lu_2P_4O_{22}]$. (b) Side view of the tunnel in the $KAlP_2O_7$-type diphosphates, β-KYP_2O_7, $ALuP_2O_7$ (A = K, Rb, Lu). (c) The top view of the septangular ring of $[RE_3P_4O_{27}]$ (RE = Y, Lu) that stacks along c-axis to form the tunnel in $KAlP_2O_7$-type diphosphates.

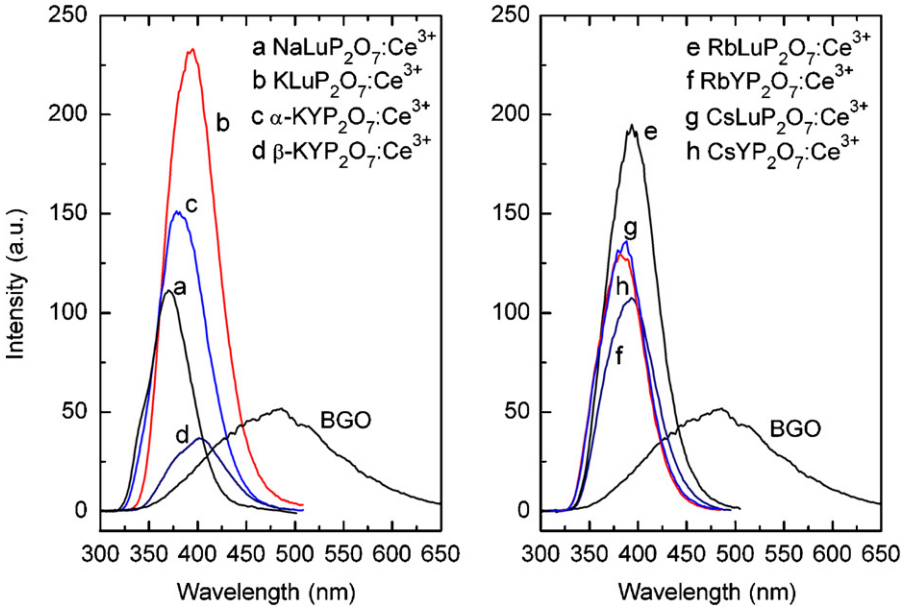

Fig. 5. X-ray excited luminescence (XEL) of Ce^{3+}-doped $AREP_2O_7$ (0.5 mol%) powder samples at room temperature. The XEL emission spectrum of $Bi_4Ge_3O_{12}$ (BGO) powder sample was given as a reference. All of the samples are measured under the same conditions.

not be attributed to the small amount of $LuPO_4$:Ce parasite phase since the observed emission peaks at 370 nm whereas the emission of $LuPO_4$:Ce peaks at 360 nm instead [20]. However, comparing with the VUV-excited emission spectra the X-ray excited Ce^{3+} emission features slight redshift due to a greater percentage of

emission from $5d \rightarrow 4f(^2F_{7/2})$ transition. The emission location in the UV/blue range matches well with commercial photomultiplier tubes and avalanche photodiodes, which makes $AREP_2O_7:Ce^{3+}$ advantageous in scintillation applications. Though large single crystals are required in the measurement of scintillation light yield, a rough estimation of light yield could be made from the XEL spectra by comparing the photomultiplier tube outputs with that of a well established scintillator, $Bi_4(GeO_4)_3$ (BGO) [21]. The powder sample of BGO used here was obtained by careful grinding large pieces of BGO single crystals in an agate mortar. By integrating the emission curves presented in Fig. 5, the light yield of $AREP_2O_7$:0.5% Ce^{3+} was estimated to be 75–200% of that of BGO (seen in Table 5). Generally, the lutetium-containing samples show larger light yield than their yttrium-containing counterparts due to the larger absorption of X-ray by lutetium atoms. Overall, the obtained values were a little smaller than that of $LuPO_4$ [20] and $A_3Lu(PO_4)_2$ measured using high quality crystals [1]. Nevertheless, current values would be underestimated since the samples are not single crystals and their X-ray absorption coefficients are smaller relative to that of BGO. The concentration quenching effect appears when the doping concentration exceeds 0.5%, indicating fast energy migration among Ce^{3+} activators.

In Fig. 6, the scintillation pulse shapes of $AREP_2O_7:Ce^{3+}$ powder samples were presented, together with their

Table 5
Comparison of several scintillation properties between some commercially available scintillators and $AREP_2O_7$:Ce (0.5 mol%) samples

	Emission max (nm)	Relative light yield (NaI:Tl = 100)[a]	Decay time (ns)[b]	ρ_{cal} (g/cm^3)	Hygroscopic
NaI:Tl	415	100	230	3.67	Yes
$Bi_4Ge_3O_{12}$	480	10	300	7.13	No
$PbWO_4$	420/450	0.3	6/15	8.3	No
Lu_2SiO_5:Ce	420	75	40	7.4	No
Gd_2SiO_5:Ce	430	20	60	6.71	No
$NaLuP_2O_7$:Ce	370	7.5	5.5(17.7%)/20.4(82.3%)	4.11	No
KYP_2O_7:Ce	380	12.5	6.7(22.6%)/23.2(77.4%)	3.11	No
$KLuP_2O_7$:Ce	394	20	6.3(14.9%)/27.2(85.1%)	3.87	No
$RbYP_2O_7$:Ce	393	8.8	8.8(14.8%)/27.8(85.2%)	3.27	No
$RbLuP_2O_7$:Ce	393	16	6.3(23.2%)/24.0(76.8%)	4.20	No
$CsYP_2O_7$:Ce	383	10	5.2(16.9%)/22.2(83.1%)	3.57	No
$CsLuP_2O_7$:Ce	383	10	4.4(14.1%)/19.8(85.9%)	4.49	No

[a]The relative light yields of $AREP_2O_7$:Ce are calculated according to that of BGO, which is about 10% of NaI:Tl.
[b]The percentage in parentheses is the intensity percentage of the fast/slow emission component.

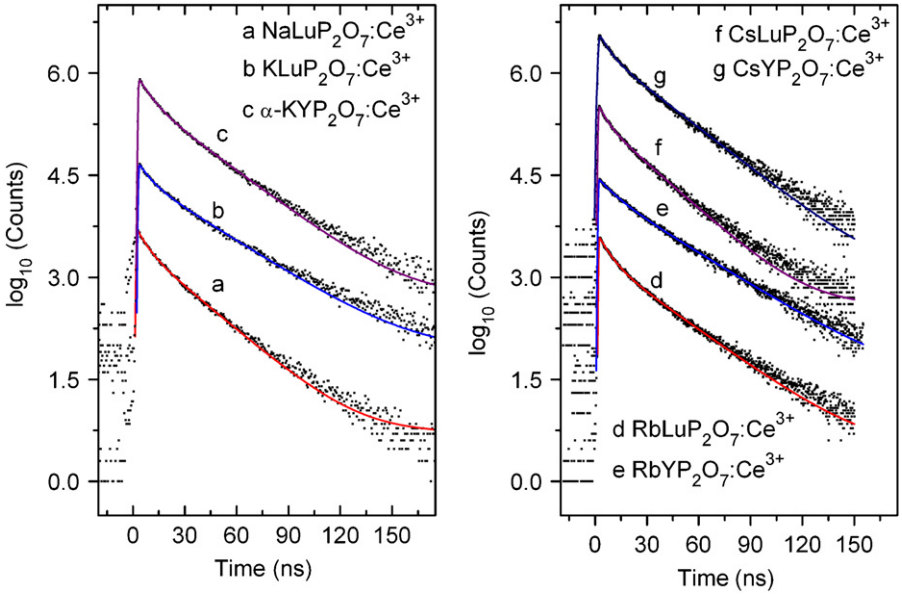

Fig. 6. Room temperature scintillation pulse shapes of Ce^{3+}-doped $AREP_2O_7$ (0.5 mol%) powder samples. Two-exponential decay fits curves were also presented (solid line). The curves have been lifted vertically for clarity. The scintillation pulse of β-$KYP_2O_7:Ce^{3+}$ was not presented due to its very low light yield comparing with the other seven diphosphates.

two-exponential decay fit curves. A two-exponential decay fit was required for a reliable reconstruction of all of the experimental data. The decay times (τ_1, τ_2) and relative intensity (I_1, I_2) of both slow and fast component were listed in Table 5. As shown in Table 5, the $AREP_2O_7$:Ce^{3+} powder samples feature a fast decay component with decay time of 4–9 ns and a slower decay component with decay time of 20–28 ns, which would be valuable in high counting rate scintillation applications. It should be pointed out that the scintillation pulse shape parameters were calculated assuming the absence of slower decay component, and it cannot be excluded that weak slow emission components would hide in the measurement background. The high similarity in both decay time and relative intensity of the slow and fast components in each sample again demonstrates their structural and compositional resemblance and suggests the same scintillation mechanism in the series of $AREP_2O_7$:Ce^{3+} samples.

For typical Ce^{3+}-activated scintillators where different exponential decay components not only arise from multi-positions of Ce^{3+} activators but also from other factors, such as charge carrier trapping, host emission and non-radiative process. For "ideal" Ce^{3+} ion that is free from any energy loss, the parity-allowed 5d–4f transition follows single-exponential decay mode with decay time τ_r that directly relates to the emission wavelength λ, $\tau_r = 1.35 \times 10^5 \lambda^2 [n(n^2+2)^2 f]^{-1}$, where n is refractive index and f is oscillator strength [1,22]. By applying the data ($n = 1.7$, $f = 13.1 \times 10^{-3}$) suggested by Lempicki and Wojtowicz [22], the theoretical decay time of $AREP_2O_7$:Ce^{3+} is estimated to be within 35–40 ns, which is apparently longer than the observed decay time in Table 5. The shortening of decay time in $AREP_2O_7$:Ce^{3+} system probably originates from considerable energy loss to non-radiative centers [23], for example grain boundaries and residual Ce^{4+} centers. The non-radiative energy loss would lead to a notable reduction in light yield, as demonstrated in the low light yield of β-KYP_2O_7:Ce sample that was not completely reduced (Fig. 5). Nevertheless, this type of defect-induced decay time shortening would be valuable in cases where fast decay is more important than light yield. Higher light yield and longer decay time are expected if large pieces of high quality single crystals are fabricated.

In the end, some scintillation properties of $AREP_2O_7$:Ce^{3+} are compared with that of several established inorganic scintillators (Table 5). As shown in Table 5, $AREP_2O_7$:Ce^{3+} show promising scintillation properties, especially for $KLuP_2O_7$:Ce^{3+} and $RbLuP_2O_7$:Ce^{3+}. Though the densities are relatively low, considering their short decay time, high light yield and non-hygroscopic nature, these materials would be potential candidates in scintillation applications under not too high-energy radiation.

4. Conclusion

In this work, the crystal structure data of five $AREP_2O_7$-type alkali rare earth diphosphates were obtained from Rietveld refinement of powder XRD patterns, including the $NaYbP_2O_7$-type $NaLuP_2O_7$ ($P2_1/n$, $Z = 4$) and four $KAlP_2O_7$-type β-KYP_2O_7 and $ALuP_2O_7$ (A = K, Rb, Cs) ($P2_1/c$, $Z = 4$). By doping with Ce^{3+} activators, the series of $AREP_2O_7$:Ce^{3+} samples show strong emission in the UV-blue region with high light yields (1–2 times of BGO) and short decay times (20–28 ns), which would be promising in high-counting rate scintillation applications under not too high energy radiation. The relatively short decay time probably originates from defect-induced non-radiative deactivation of Ce^{3+} ions.

Acknowledgments

This work was supported by the Key Project (50332050) from the NNSF of China and the 100 Talents Program from the Chinese Academy of Sciences and fund for Young Leading Researchers from Shanghai municipal government. We also thank Prof. Liang Fang for his kindly help in collecting XRD patterns for Rietveld refinement.

Reference

[1] D. Wisniewski, A.J. Wojtowicz, W. Drozdowski, J.M. Farmer, L.A. Boatner, Cryst. Res. Technol. 38 (2003) 275.
[2] A. Jouini, J.C. Gâcon, M. Ferid, M. Trabelsi-Ayadi, Opt. Mater. 24 (2003) 175.
[3] J.L. Yuan, J. Wang, D.B. Xiong, J.T. Zhao, Y.B. Fu, G.B. Zhang, C.S. Shi, J. Lumin. 126 (2007) 717.
[4] J.J. Carvajal, I. Parreu, R. Sole, X. Solans, F. Diaz, M. Aguilo, Chem. Mater. 17 (2005) 6746.
[5] G. Vitins, Z. Kanepe, A. Vitins, J. Ronis, A. Dindune, A. Lusis, J. Solid State Electrochem. 4 (2000) 146.
[6] N. Khay, A. Ennaciri, M. Harcharras, Vib. Spectrosc. 27 (2001) 119.
[7] A. Hamady, T. Jouini, Acta Crystallogr. C 52 (1996) 2949.
[8] M. Ferid, K. Horchani-Naifer, M. Trabelsi-Ayedi, Z. Kristallogr. NCS 219 (2004) 353.
[9] K. Horchani-Naifer, M. Ferid, Solid State Ionics 176 (2005) 1949.
[10] A. Hamady, M. Faouzi Zid, T. Jouini, J. Solid State Chem. 113 (1994) 120.
[11] M.-R. Li, W. Liu, H.-H. Chen, X.-X. Yang, Z.-B. Wei, D.-H. Cao, M. Gu, J.-T. Zhao, Eur. J. Inorg. Chem. (2005) 4693.
[12] J.L. Yuan, X.J. Wang, D.B. Xiong, C.J. Duan, J.T. Zhao, Y.B. Fu, G.B. Zhang, C.S. Shi, J. Lumin. 126 (2007) 130.
[13] C.W.E. van Eijk, Nucl. Instrum. Meth. A 460 (2001) 1.
[14] H.N. Ng, C. Calvo, Can. J. Chem. 51 (1973) 2613.
[15] A. Akrim, D. Zambon, J. Metin, J.C. Cousseins, Eur. J. Inorg. Chem. 30 (1993) 483.
[16] J. Rodriguez-Carvajal, FULLPROF version July 2006, ILL, unpublished.
[17] M. Gabelica-Robert, M. Goreaud, P. Labbe, B. Raweau, J. Solid State Chem. 45 (1982) 389.
[18] H. Hong, Mater. Res. Bull. 11 (1976) 173.
[19] A. Bessiere, P. Dorenbos, C.W.E. van Eijk, K.W. Kramer, H.U. Gudel, C. de Mello Donega, A. Meijerink, Nucl. Instrum. Meth. A 537 (2005) 22.
[20] A. Lempicki, E. Berman, A.J. Wojtowicz, M. Balcerzyk, IEEE Trans. Nucl. Sci. 40 (1993) 384.
[21] S.E. Derenzo, W.W. Moses, J.L. Cahoon, R.C.C. Perera, IEEE Trans. Nucl. Sci. 37 (1990) 203.
[22] A. Lempicki, A.J. Wojtowicz, J. Lumin. 60–61 (1994) 942.
[23] P.A. Rodnyi, Radiat. Meas. 33 (2001) 605.